

Plasmonically enhanced spectrally selective narrowband MWIR and LWIR light detection based on hybrid nanopatterned graphene and phase changing vanadium oxide heterostructure operating close to room temperature

Muhammad Waqas Shabbir⁽¹⁾, Sayan Chandra⁽²⁾, and Michael N. Leuenberger^{(1,3)*}

⁽¹⁾ *NanoScience Technology Center and Department of Physics,
University of Central Florida, Orlando, FL 32826, USA.*

⁽²⁾ *Department of Physics and Astronomy, Appalachian State University, Boone, NC 28608, USA.*

⁽³⁾ *College of Optics and Photonics, University of Central Florida, Orlando, FL 32826, USA.*

We present the model of an ultrasensitive mid-infrared (mid-IR) photodetector operating in the mid-wavelength infrared (MWIR) and long-wavelength infrared (LWIR) domains consisting of a hybrid heterostructure made of nanopatterned graphene (NPG) and vanadium dioxide (VO₂) which exhibits a large responsivity of $R \sim 10^4$ V/W, a detectivity exceeding $D^* \sim 10^{10}$ J, and a sensitivity in terms of noise-equivalent power $NEP \sim 100$ fW/ $\sqrt{\text{Hz}}$ close to room temperature by taking advantage of the phase change of a thin VO₂ film. Our proposed photodetector can reach an absorption of nearly 100% in monolayer graphene due to localized surface plasmons (LSPs) around the patterned circular holes. The geometry of the nanopattern and an electrostatic gate potential can be used to tune the absorption peak in the mid-IR regime between 3 and 12 μm . After the photon absorption by the NPG sheet and the resulting phase change of VO₂ from insulating to metallic phase the applied bias voltage V_b triggers a current through the VO₂ sheet, which can be detected electronically in about 1 ms, shorter than the detection times of current VO₂ bolometers. Our envisioned mid-IR photodetector reaches detectivities of cryogenically cooled HgCdTe photodetectors and sensitivities larger than VO₂ microbolometers while operating close to room temperature.

KEYWORDS: Localized surface plasmons, graphene, absorbance, vanadium dioxide, photodetection, bolometer.

Due to the low photon energy of IR radiation cryogenic cooling is required for highly sensitive photodetection based on low band gap materials like mercury-cadmium-telluride (HgCdTe). Various kinds of microbolometers primarily based on vanadium oxide (VOx) offer uncooled detection of IR radiation. However, microbolometers suffer from low sensitivity, slow response and tedious multi-step complex lithographic processes [1]. Photodetection based on the bolometric effect takes advantage of the dependence of the resistivity on the temperature to detect incident light, typically in the infrared regime. Vanadium oxide (VO₂) has become one of the standard materials for building microbolometers with broadband mid-IR photodetection because it features a reversible insulator-to-metal phase transition (IMT) when heated above the phase transition temperature T_c , which is slightly above and close to room temperature [2]. Bulk VO₂ undergoes a phase transition from an insulating state with monoclinic crystal structure below 68°C to a metallic state with rutile crystal structure above $T_c = 68^\circ\text{C}$ ($=341$ K) [3–5]. This phase transition is fully reversible with a hysteresis loop, occurs on a subpicosecond timescale [6, 7], and can be initiated either thermally, electrically [8], or optically [9]. While for bulk VO₂ optically induced IMT can only be achieved by pumping above the band gap of $E_g = 670$ meV of bulk VO₂, it is possible to induce IMT in thin films at energies of 200 meV and above (corresponding to wavelengths of $\lambda = 6.2$ μm and below) due to electronic defects inside the band gap [10], which is the reason why VO₂ thin films can be used for IR detection

in a wide IR range, in particular in the 3–5 μm range. Interestingly, when VO₂ is in the form of a thin film, its transition temperature T_c depends strongly on the thickness d of the film, i.e. T_c decreases from 65°C ($=338$ K) for $d = 25$ nm down to 52°C ($=325$ K) for $d = 3$ nm [11]. While IR radiation with wavelengths above about $\lambda = 1$ μm cannot detect the change in thickness of around 20 nm, it certainly distinguishes between the insulating and the metallic phase of VO₂. All these properties make VO₂ the ideal material for developing mid-IR photodetectors based on the IMT effect.

However, photodetection of mid-IR light with wavelength above about 6 μm is inefficient with VO₂ bulk or thin films because of the relatively weak interaction between the incident photons and the optical phonons in VO₂. This interaction is so weak that the IMT cannot be achieved. That is why in the wavelength regime of 8 to 12 μm the photodetection is based purely on the bolometric effect in the semiconducting phase of VO₂ [13, 14]. Here, by adding a single layer of nanopatterned graphene (NPG) on top of a layer of VO₂, we present the model of a photodetector that not only greatly enhances the absorption of mid-IR light energy in the longer wavelength regime from $\lambda = 6$ μm and exceeding 12 μm but also narrows the absorption bandwidth to 0.1 μm within the mid-IR range of 3 to 12 μm , thereby enabling plasmonically enhanced spectrally selective absorption of mid-IR light for the IMT effect in a heterostructure made of NPG and VO₂.

Building upon the knowledge we acquired for develop-

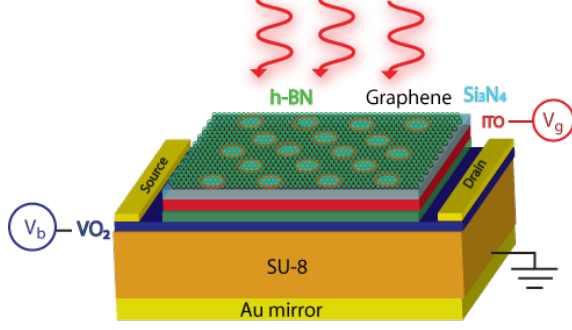


Figure 1. Schematic showing our proposed IMT-based mid-IR light photodetector consisting of hybrid NPG-VO₂. The materials from top to bottom are: 1 single layer of hexagonal boron nitride (h-BN), for preventing oxidation of graphene at higher temperatures (*), 1 single layer of patterned graphene (*), 65 nm of Si₃N₄ (*), for large n-doping and gating, 65 nm of ITO (*), metallic contact for gating, which is also transparent in mid-IR, 20 nm of h-BN (*), used for efficient heat transfer, 3 nm of VO₂ (*), contacted with source and drain Au leads, $\lambda/4n_{\text{SU8}}$ of SU8,[12] which is transparent in mid-IR, and Au back mirror. $n_{\text{SU8}} = 1.56$ is the refractive index of SU8. All the layers marked with an asterisk (*) are patterned with the same hexagonal lattice of holes.

ing spectrally selective photodetectors made of NPG that detect mid-IR light by means of the photothermoelectric effect [12, 15, 16] and the knowledge we acquired for developing thermal emitters based on NPG [17], we develop here the model of a mid-IR microbolometer that consists of an hexagonal boron nitride (h-BN) coated NPG, silicon nitride (Si₃N₄), indium tin oxide (ITO), VO₂, polymer, and gold (Au) mirror, as shown in Fig. 1. The main working principle of our envisioned mid-IR photodetector can be summarized as follows. After mid-IR photons get absorbed by the NPG sheet at a wavelength that matches the localized surface plasmon (LSP) resonance, the NPG's temperature increases and transfers the heat through the Si₃N₄ and ITO layers to the VO₂ layer. By patterning not only the graphene sheet but also the Si₃N₄ and ITO layers we maximize the heat transfer to the VO₂ layer. Once the VO₂ layer's temperature increases above the phase transition temperature T_c , the VO₂ layer undergoes a transition from insulating to metallic phase. The patterning of the VO₂ layer decreases its volume, thereby decreasing the heat required to drive the VO₂ layer over T_c , which in turn increases the sensitivity (NEP) of our proposed NPG-VO₂ photodetector. During this whole time a bias voltage V_b is applied to the VO₂ layer, which upon phase transition triggers a current through the VO₂ layer, which can be detected electronically in about 1 ms, shorter than the

detection time of typical VO₂ bolometers [14].

For the electronic response of the graphene sheet and the VO₂ layer to the incident mid-IR photons, we need to consider the intraband conductivity of graphene and the dielectric function of VO₂ in the insulating and metallic regimes. Using the linear dispersion relation, the intraband optical conductivity of graphene is [12, 18]

$$\sigma_{\text{intra}}(\omega) = \frac{e^2}{\pi\hbar^2} \frac{2k_B T}{\tau^{-1} - i\omega} \ln \left[2 \cosh \left(\frac{E_F}{2k_B T} \right) \right], \quad (1)$$

which in the case of $E_F \gg k_B T$ is reduced to

$$\sigma_{\text{intra}}(\omega) = \frac{e^2}{\pi\hbar^2} \frac{E_F}{\tau^{-1} - i\omega} = \frac{2\varepsilon_m \omega_p^2}{\pi\hbar^2(\tau^{-1} - i\omega)}, \quad (2)$$

where τ is determined by impurity scattering and electron-phonon interaction $\tau^{-1} = \tau_{\text{imp}}^{-1} + \tau_{\text{e-ph}}^{-1}$. Using the mobility μ of the NPG sheet, it can be presented in the form $\tau^{-1} = ev_F^2/(\mu E_F)$, where $v_F = 10^6$ m/s is the Fermi velocity in graphene. $\omega_p = \sqrt{e^2 E_F / 2\varepsilon_m}$ is the bulk graphene plasma frequency.

The dielectric function of VO₂ can be approximated by means of a constant for the insulating phase [19],

$$\epsilon_i = \epsilon_\infty, \quad (3)$$

and by means of the Drude formula for the metallic phase,

$$\epsilon_m(\omega) = \epsilon_\infty - \frac{\Omega_p^2}{\omega(\omega + i\Gamma)} \left(1 + \frac{ic\Gamma}{\omega + i\Gamma} \right), \quad (4)$$

where $\Omega_p = \sqrt{Ne^2/\epsilon_0 m^*}$ is the plasma frequency of VO₂, $\Gamma = e/m^* \mu_{\text{VO}_2}$ is the scattering rate in VO₂, with $\mu_{\text{VO}_2} = 2$ cm²/Vs being the mobility in VO₂, $N = 1.3 \times 10^{22}$ cm⁻³ the free-carrier concentration in VO₂, and $m^* = 2m_e$ the effective mass of the charge carriers in VO₂. m_e is the free electron mass. c is the fraction of the original velocity of the electron after scattering.

We used the finite-difference time domain method (FDTD) to calculate the absorbance of the hybrid NPG-VO₂ photodetector as shown in Fig. 2 (a) when VO₂ is in the insulating phase and in Fig. 2 (c) when VO₂ is in the metallic phase. The resonance peaks due to the absorption of mid-IR light by localized surface plasmons (LSPs) in NPG are clearly visible and similar to the ones found in Refs. [12, 15–17]. The main difference is that the VO₂ layer exhibits very low absorbance (around 6%) of mid-IR light in the insulating phase but a larger broadband absorption in the metallic phase. The thicker the metallic VO₂ layer is, the stronger is the absorption of mid-IR light. We chose a VO₂ layer thickness of 3 nm for two important reasons: Firstly, a thinner VO₂ layer results in weaker absorption and thus makes it easier for the photodetector to cool down after the incident mid-IR radiation is turned off. Secondly, the thinner VO₂ layer has

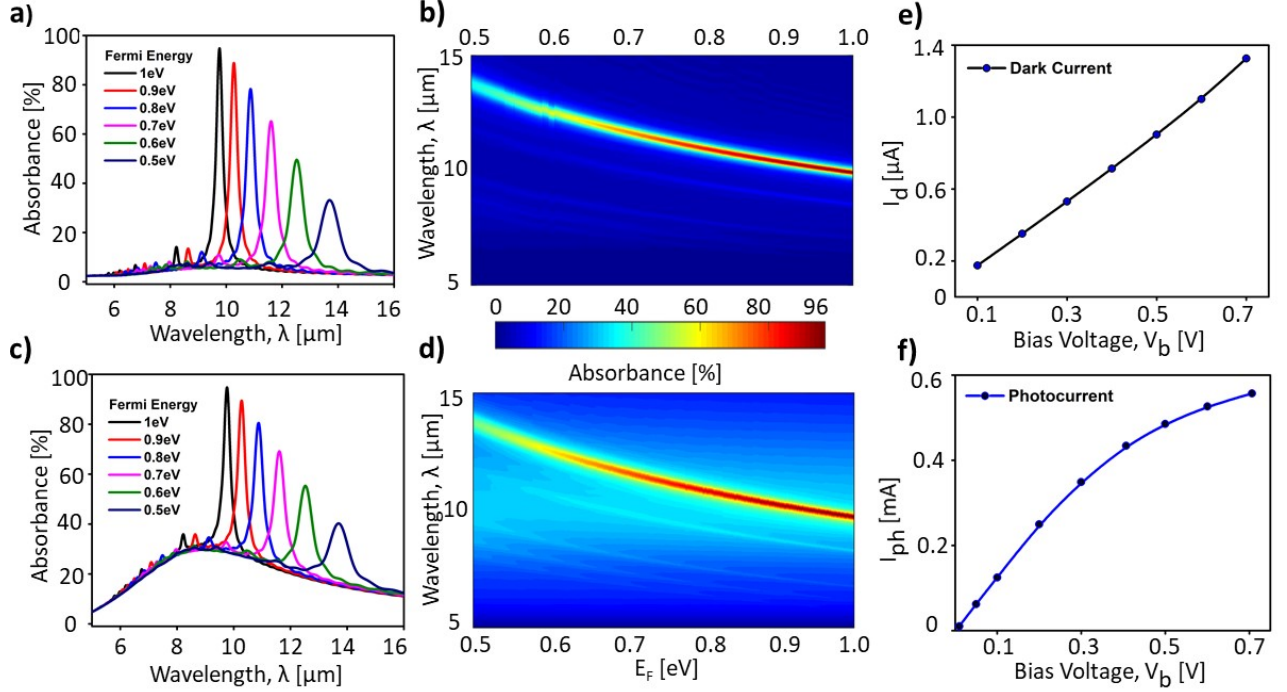


Figure 2. Absorbance and photocurrent of the NPG-VO₂ photodetector shown in Fig. 1 with nanopattern made of a hole diameter of 300 nm and a period of 450 nm. (a) Absorbance when VO₂ is in the insulating phase, calculated by means of the FDTD method. The resonance peaks of the LSP are clearly visible and tunable by means of a gate voltage that shifts the Fermi energy inside the NPG sheet. Absorbance of mid-IR light in this wavelength regime in insulating VO₂ is very low. (b) Absorbance as a function of wavelength and Fermi energy, showing the overall tunability of the LSP resonance peaks, when VO₂ is in the insulating phase. (c) Absorbance of the NPG-VO₂ photodetector shown in Fig. 1 when VO₂ is in the metallic phase. The resonance peaks of the LSP are still clearly visible and tunable by means of a gate voltage that shifts the Fermi energy inside the NPG sheet. Compared with the absorbance for insulating VO₂ shown in (a), the metallic VO₂ layer absorbs mid-IR light over a large wavelength regime and exhibits a maximum of about 30% at a wavelength of about $\lambda = 9 \mu\text{m}$. (d) Absorbance as a function of wavelength and Fermi energy, showing the overall tunability of the LSP resonance peaks, when VO₂ is in the metallic phase. (e) $I_{\text{ph}} - V_b$ characteristics of the NPG-VO₂ photodetector for insulating VO₂. Note that the scale of the current is given in μA and is thus very small compared to the photocurrent for metallic VO₂ shown in (f). (f) $I_{\text{ph}} - V_b$ characteristics of the NPG-VO₂ photodetector for metallic VO₂. Note that the scale of the current is given in mA and is thus very large compared to the photocurrent for insulating VO₂ shown in (e).

a lower phase transition temperature of $T_c = 52^\circ\text{C}$ ($=325 \text{ K}$) and thus requires less external heating for keeping the photodetector at an optimum operating temperature (see below).

The absorbance resonance peak as a function of wavelength can be tuned by means of the Fermi energy of NPG, as shown in Fig. 2 (b) when VO₂ is in the insulating phase and in Fig. 2 (d) when VO₂ is in the metallic phase. Thus, the gate voltage allows the operating wavelength of the VO₂-NPG photodetector to be tuned in addition to the size and period of the nanopattern in graphene.

For modeling the operation of the proposed NPG-VO₂ mid-IR photodetector, we used COMSOL and the following theory for the thermoelectric properties of VO₂ close to the phase transition temperature T_c . The VO₂ layer is

operated around the IMT phase transition temperature T_c . The performance of the bolometric detection can be analyzed by means of the heat equation and a hysteresis model [20]. The heat equation reads

$$C \frac{dT}{dt} = \alpha P + I^2 R(T) - G(T - T_h), \quad (5)$$

where C is the heat capacity, α is the absorbance, P is the power of the incident radiation, I is the time-independent bias current, $R(T)$ is the temperature-dependent resistance, G is the thermal conductivity of the heat sink, and T_h is the time-independent temperature of the heat sink. The hysteretic behavior of $R(T)$ for VO₂ layer can be calculated by

$$R(T) = 17 \exp\left(\frac{2553}{T + 273}\right) g(T) + 140, \quad (6)$$

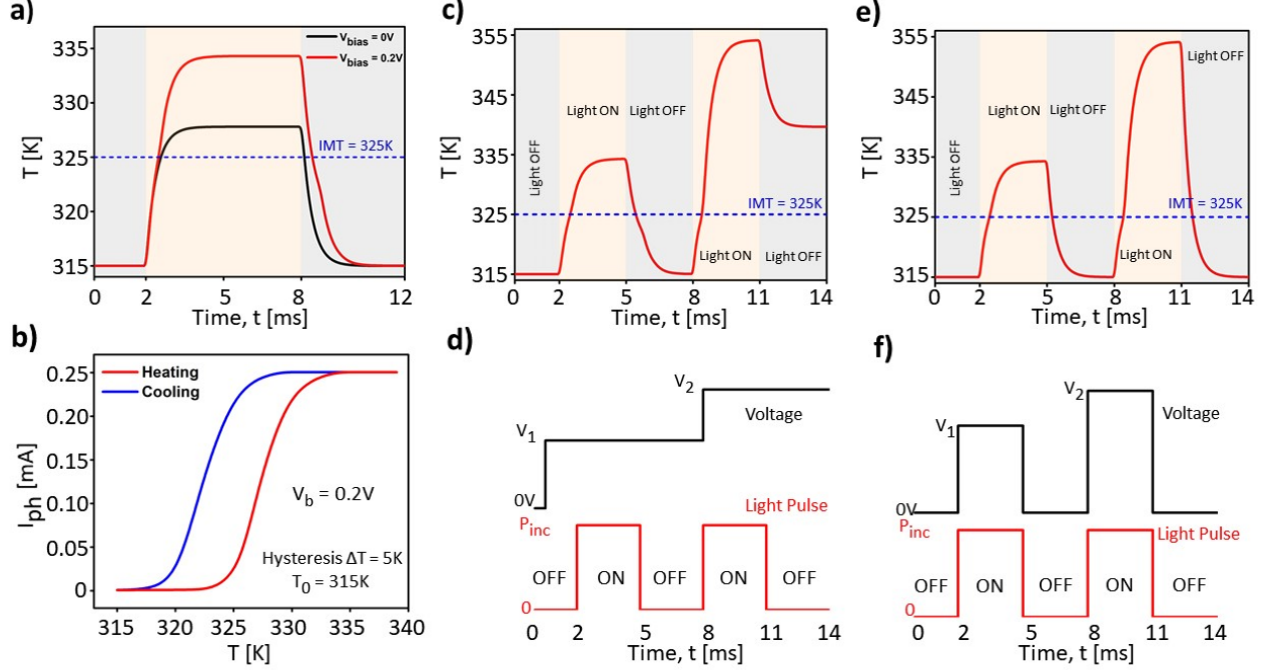


Figure 3. Photocurrent as functions of temperature and time of the NPG-VO₂ photodetector shown in Fig. 1 with nanopattern made of a hole diameter of 300 nm and a period of 450 nm. (a) Temperature T of the VO₂ layer as a function of time, showing the photodetection process while the incident mid-IR light is turned on at time $t = 2$ ms and subsequently turned off at time $t = 8$ ms for constant applied bias voltages $V_b = 0$ (black curve) and $V_b = 0.2$ V (red curve). (b) Photocurrent I_{ph} through the VO₂ layer as a function of Temperature T for a constant applied bias voltage $V_b = 0.2$ V during the heating (red curve) and cooling (blue curve) process. The base temperature of the substrate is kept at $T_0 = 315$ K. The temperature difference of the hysteresis is $\Delta T = 5$ K. (c) Temperature T of the VO₂ layer as a function of time for two constant values of the bias voltages $V_b = 0.2$ V and $V_b = 0.25$ V. (d) Bias voltage V_b as a function of time t .

where the semiconductor volume fraction is given by

$$g(T) = \frac{1}{2} + \frac{1}{2} \tanh \beta \left[\delta \frac{w}{2} + T_c - \left(T + T_{pr} P \left(\frac{T - T_r}{T_{pr}} \right) \right) \right], \quad (7)$$

where w is the width of the hysteresis, β is a function of dg/dT at T_c , $P(x)$ is an arbitrary monotonically decreasing function, and $\delta = \text{sign}(dT/dt)$. The proximity temperature is given by

$$T_{pr} = \delta \frac{w}{2} + T_c - \frac{1}{\beta} \arctan h(2g_r - 1) - T_r. \quad (8)$$

Eqs. (5)-(8) provide a simple method to describe the hysteretic behavior of the plasmonically driven bolometric photodetector. The incident power P_{inc} is then given by the energy pumped into the plasmonic nanostructure.

Using this thermoelectric theory and combining it with our FDTD results, we developed a photothermoelectric theory of the NPG-VO₂ heterostructure. We present the current as a function of applied bias voltage V_b (I-V characteristics) for insulating VO₂ in Fig 2 (e). and for metallic VO₂ in Fig. 2 (f). Note that the current flows only

through VO₂, not through NPG. NPG is used only as a photothermoelectric heating element. When the incident mid-IR light is off, a very weak dark current I on the scale of μA is flowing when a bias voltage V_b is applied on the order of 0.1 to 1.0 V. In stark contrast, when the incident mid-IR light is on, a much larger light current I on the scale of mA is flowing with the same applied bias voltage V_b . This effect is due to the phase transition of VO₂ between insulating and metallic phases. We take advantage of this effect to develop the model of an ultrasensitive photodetector based on the NPG-VO₂ heterostructure.

After modeling the heating and cooling of the NPG-VO₂ heterostructure as a function of time, we identified the optimum photodetection process. The resulting temperature T of the VO₂ layer as a function of time t and the photocurrent I_{ph} through the VO₂ layer as a function of temperature T for a constant applied bias voltage $V_b = 0.2$ V are shown in Fig. 3 (a) and (b). We used the theoretical models and experimental values of conductivity, thermal conductivity, and heat capacity of VO₂

given in Refs. [21–24]. Our results reveal that the NPG-VO₂ photodetector has a response time on a time scale of the order of 1 ms, shorter than current microbolometers based on VO₂ alone [14].

The amount of Joule heating can be seen in Fig. 3(a) as the difference in temperature between the cases $V_b = 0$ V and $V_b = 0.2$ V. When the applied bias voltage V_b is kept constant and is too large, the Joule heating prevents the photodetector from cooling down, as shown in Fig. 3 (c) and (d). Such a behavior is problematic. In order to overcome this problem, one can apply a pulsed bias voltage $V_b(t)$, which ensures the cooling of the photodetector below the phase transition temperature T_h , as shown in Fig. 3 (e) and (f).

The responsivity \mathcal{R} of the NPG-VO₂ photodetector can be calculated by means of the formula [16]

$$\mathcal{R} = \frac{(I_{\text{light}} - I_{\text{dark}})R}{P_{\text{inc}}}, \quad (9)$$

where R is the resistance of VO₂ in the metallic phase, I_{light} is the light current when the incident light is on, I_{dark} is the dark current when the incident light is off, and P_{inc} is the power of the incident light. The responsivity as a function of Fermi energy E_F of NPG is shown in Fig. 4.

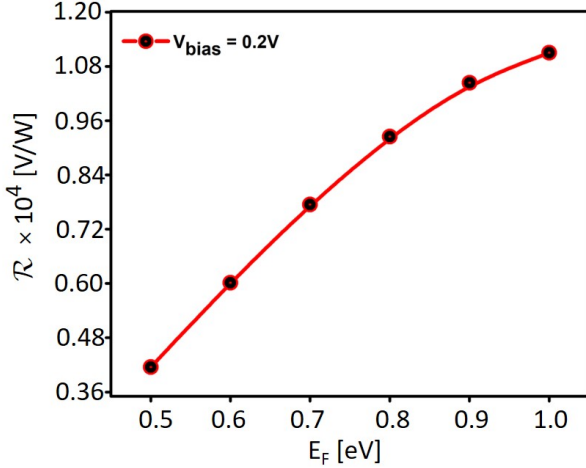


Figure 4. Responsivity of the NPG-VO₂ photodetector as a function of Fermi energy E_F of NPG.

The sensitivity of the NPG-VO₂ photodetector is determined by the noise-equivalent power NEP, being an important figure of merit for the performance of a photodetector. The NEP of a photodetector provides a measure for the minimum detectable power per 1 Hz of bandwidth. The formula for NEP reads [16]

$$\text{NEP} = \frac{\nu_n}{\mathcal{R}}, \quad (10)$$

where

$$\nu_n = \sqrt{\nu_t^2 + \nu_b^2 + \nu_f^2} \quad (11)$$

is the root-mean-square of the total noise voltage, which consists of the sum over all possible noise voltages, such as the thermal Johnson-Nyquist noise ν_t , due to thermal motion of the charge carriers and independent of the bias voltage V_b , the shot noise ν_b , due to the discrete nature of uncorrelated charge carriers, and the $1/f$ noise ν_f , also called flicker noise, due to random resistance fluctuations. The Johnson noise is given by [25]

$$\nu_t = \sqrt{4k_B T R}, \quad (12)$$

where k_B is the Boltzmann constant, T is the temperature, and R is the resistance. The shot noise is given by [25]

$$\nu_b = \sqrt{2eI_d R^2}, \quad (13)$$

where e is the elementary charge and I_d is the dark current. Since the dark current is very low and the NPG-VO₂ photodetector operates close to room temperature, the shot noise is much smaller than the Johnson noise. Therefore, we can safely neglect the shot noise. At a modulation frequency of V_b of around 1 kHz we can also neglect the $1/f$ noise. Using the NEP, we can calculate the detectivity of the NPG-VO₂ photodetector by means of the formula [16]

$$D^* = \frac{\sqrt{A}}{\text{NEP}}, \quad (14)$$

where A is the area of the photodetector. The results of these figures of merit are shown in Table I. By increasing the substrate temperature T_0 , it is possible to decrease the hysteresis temperature difference ΔT , which in turn results in an enhanced sensitivity NEP and a larger detectivity D^* . The details of these additional results are shown in the supplementary material.

ΔT [K]	P [μ W]	T_0 [K]	\mathcal{R} [V/W]	NEP [fW/ $\sqrt{\text{Hz}}$]	D^* [Jones]
5.0	18.0	315.0	1.1×10^4	347	0.50×10^{10}
3.0	14.0	317.0	1.4×10^4	273	0.64×10^{10}
1.2	10.6	318.8	1.9×10^4	203	0.85×10^{10}

Table I. Figures of Merit of the NPG-VO₂ photodetector.

Table I shows that the detectivity D^* of the NPG-VO₂ photodetector operating close to room temperature is close to D^* of cryogenically cooled HgCdTe photodetectors. The NPG-VO₂ photodetector reaches a sensitivity close to VO₂ microbolometers while exhibiting a shorter detection time of around 1 ms and being able to detect photons also in the LWIR regime, which is impossible for VO₂ microbolometers.

Since we want to realize a linear dependence of the photocurrent I_{ph} as a function of input power P_{inc} of the mid-IR light, we add a gradient in the thickness of the

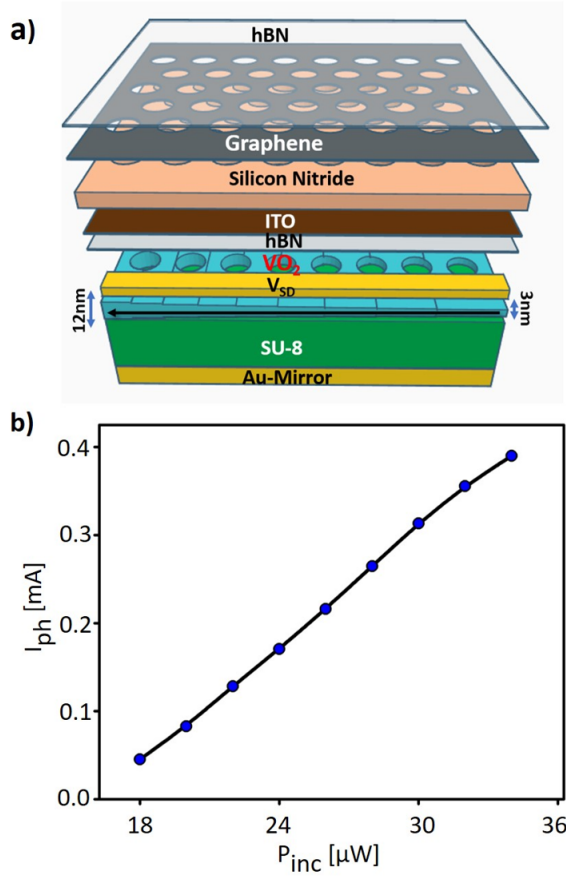


Figure 5. (a) Illustration of NPG-VO₂ photodetector with a VO₂ layer whose thickness has a gradient varying from 3 nm to 12 nm. (b) Photocurrent I_{ph} as a function of input power P_{inc} of the mid-IR light for the photodetector shown in (a), which is linear due to the gradient in the thickness of the VO₂ layer.

VO₂ layer as shown in Fig. 5 (a), i.e. the VO₂ layer thickness is varied from 3 nm to 12 nm. The resulting linear photocurrent I_{ph} as a function of input power P_{inc} is shown in Fig. 5 (b). Indeed, the photocurrent I_{ph} is now linear as a function of the input power P_{inc} , which provides an optimized mapping of P_{inc} onto I_{ph} for maximum dynamic range.

In conclusion, we present the model of an ultrasensitive mid-infrared (mid-IR) photodetector based on a heterostructure made of NPG and VO₂, thereby extending the responsivity of a VO₂ microbolometer to the LWIR domain. Moreover, this hybrid NPG-VO₂ photodetector has a narrowband absorption in the MWIR and LWIR that can be tuned by means of a gate voltage. Our results show that the NPG-VO₂ photodetector can reach a large responsivity $R \sim 10^4$ V/W, a detectivity $D^* \sim 10^{10}$ Jones, and a sensitivity in terms of NEP $NEP \sim 100$ fW/ $\sqrt{\text{Hz}}$ close to room temperature by taking advantage of the phase change of a thin

VO₂ layer. The NPG sheet achieves an absorption of nearly 100% due to localized surface plasmons (LSPs) around the patterned circular holes in a hexagonal lattice symmetry. The electrostatic gate potential can be used to tune the wavelength peak in the MWIR and LWIR regimes between 3 and 12 microns, thereby overcoming the intrinsic upper limit of 6 microns for microbolometers based on VO₂. Our COMSOL simulations show that the NPG-VO₂ photodetector is able to operate on a time scale of 1 ms, much shorter than the response times of current microbolometers based on VO₂ alone. Our proposed mid-IR photodetector reaches detectivities of cryogenically cooled HgCdTe photodetectors and sensitivities close to and field of view similar to VO₂ microbolometers while operating close to room temperature.

We acknowledge support from NSF CISE-1514089.

SUPPLEMENTARY INFORMATION

In order to show that NPG is absolutely required to achieve mid-IR photodetection in the wavelength range of $\lambda = 3 \mu\text{m}$ to $12 \mu\text{m}$ as presented in this paper, we also calculated the absorbance and photocurrent for the cases (i) when graphene, Si₃N₄, and ITO are absent, (ii) when graphene is absent, and (iii) when graphene is not patterned. These results are compared with (iv) results for the NPG-VO₂ photodetector shown in Fig. 1. All these results are shown in Table II in the case of $V_{bias} = 0.2$ V, base temperature $T_0 = 315$ K, incident radiation power $P_{inc} = 18 \mu\text{W}$, wavelength $\lambda = 9.76 \mu\text{m}$, and VO₂ thickness of 3 nm.

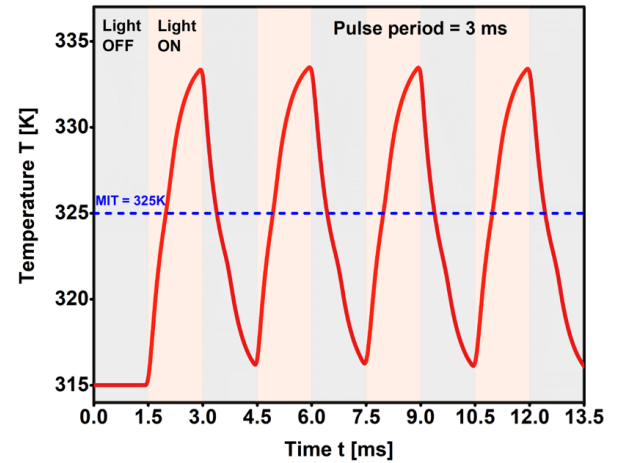


Figure 6. Temperature T of the NPG-VO₂ photodetector as a function of time t under pulsed mid-IR light illumination with period $\tau = 3$ ms.

Geometry	T_{\max} [K]	I_{dark} [mA]	I_{light} [mA]	I_{ph} [mA]
(i)	316.8	0.35×10^{-3}	0.369×10^{-3}	0.019×10^{-3}
(ii)	317.4	0.35×10^{-3}	0.376×10^{-3}	0.026×10^{-3}
(iii)	317.7	0.35×10^{-3}	0.381×10^{-3}	0.031×10^{-3}
(iv)	334.3	0.35×10^{-3}	0.25	0.25

Table II. Comparison between geometries (i), (ii), (iii) without NPG and (iv) with NPG.

It can be seen from Table II that the cases (i) to (iii) achieve only a small photocurrent, in stark contrast to case (iv) that takes advantage of NPG. The reason for this large difference is the low absorbance of the structures (i) to (iii), as shown in Fig. 7.

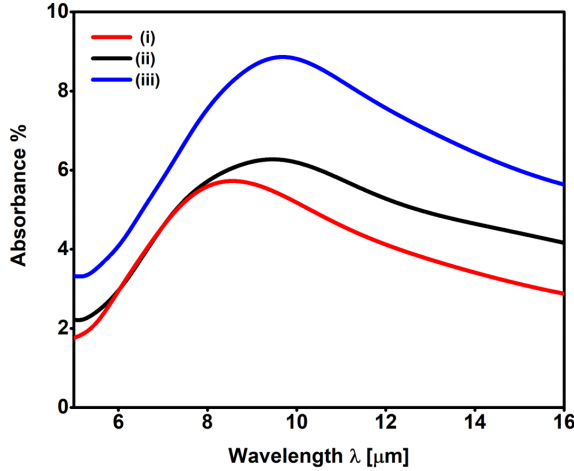


Figure 7. Absorbance as a function of wavelength λ for the cases (i) when graphene, Si_3N_4 , and ITO are absent, (ii) when graphene is absent, and (iii) when graphene is not patterned. These absorbances are much smaller than for case (iv) that takes advantage of NPG, as shown in Fig. 2.

In order to study the response of the NPG- VO_2 photodetector on a train of incident light pulses, we calculate the temperature T as a function of time t with pulse period $\tau = 3$ ms. The result is shown in Fig. 6. Thus, the response time of the NPG- VO_2 photodetector is of the order of 1 ms.

If the hysteresis curve of the photocurrent as a function of temperature can be made narrower with respect to the temperature T [26], then it is possible to increase the base temperature of the substrate T_0 . In that case, it is possible to reduce the required temperature difference ΔT for triggering the phase transition, which in turn allows us to also decrease the bias voltage V_b , thereby reducing the generated Joule heating power P_J inside

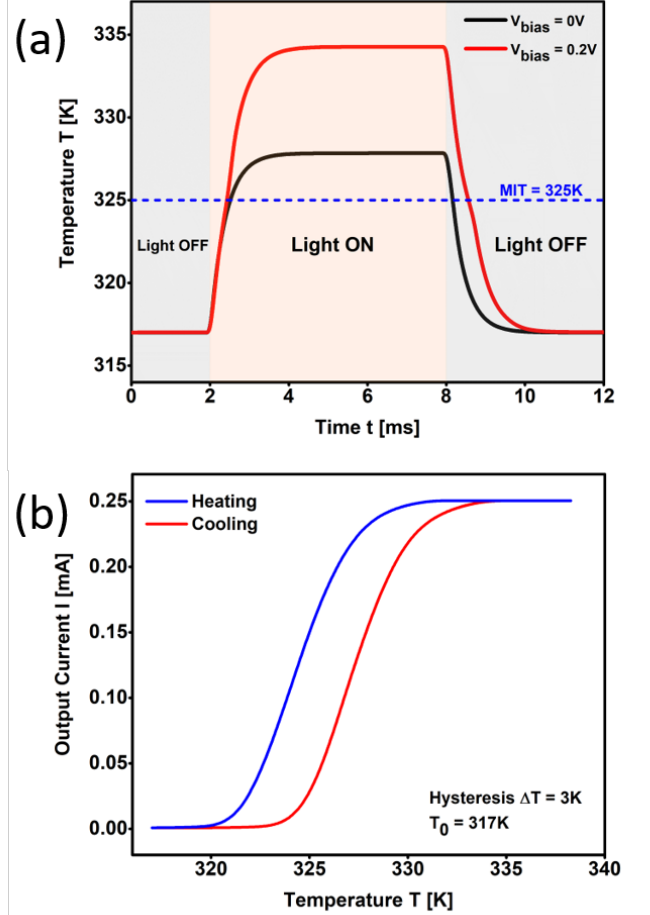


Figure 8. (a) Temperature T of the VO_2 layer as a function of time, showing the photodetection process while the incident mid-IR light is turned on at time $t = 2$ ms and subsequently turned off at time $t = 8$ ms for constant applied bias voltages $V_b = 0$ (black curve) and $V_b = 0.2$ V (red curve). (b) Photocurrent I_{ph} through the VO_2 layer as a function of Temperature T for a constant applied bias voltage $V_b = 0.2$ V during the heating (red curve) and cooling (blue curve) process. The base temperature of the substrate is kept at $T_0 = 317$ K. The temperature difference of the hysteresis is $\Delta T = 3$ K.

metallic VO_2 . The temperature T of VO_2 as a function of time t and the resulting photocurrent I_{ph} as a function of temperature for $T_0 = 317$ K and $\Delta T = 3.0$ K is shown in Fig. 8, and for $T_0 = 319$ K and $\Delta T = 1.2$ K is shown in Fig. 9.

* michael.leuenberger@ucf.edu

- [1] A. Rogalski, *Infrared Physics & Technology* **43**, 187 (2002).
- [2] A. Rogalski, *Infrared Physics & Technology* **54**, 136

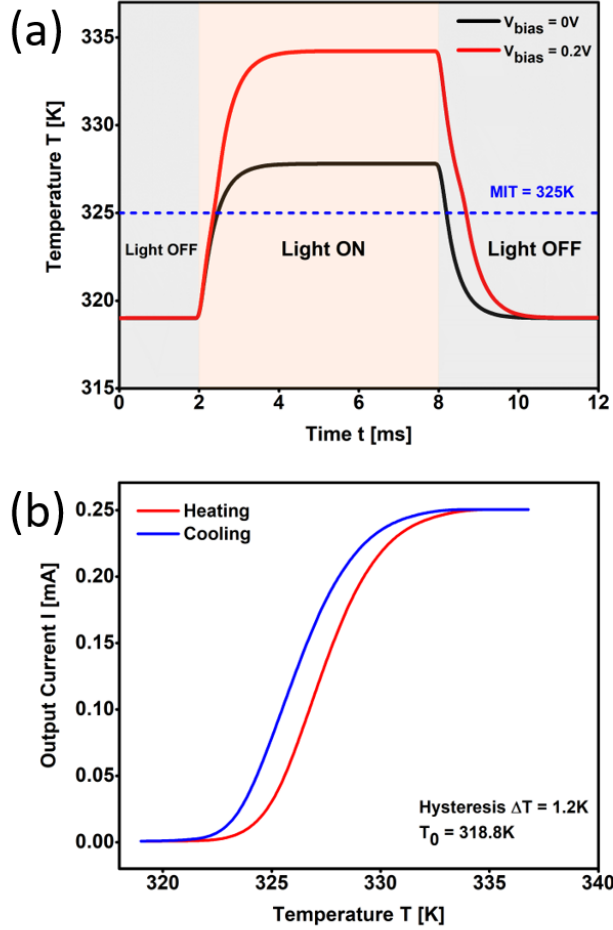


Figure 9. (a) Temperature T of the VO_2 layer as a function of time, showing the photodetection process while the incident mid-IR light is turned on at time $t = 2$ ms and subsequently turned off at time $t = 8$ ms for constant applied bias voltages $V_b = 0$ (black curve) and $V_b = 0.2$ V (red curve). (b) Photocurrent I_{ph} through the VO_2 layer as a function of Temperature T for a constant applied bias voltage $V_b = 0.2$ V during the heating (red curve) and cooling (blue curve) process. The base temperature of the substrate is kept at $T_0 = 319$ K. The temperature difference of the hysteresis is $\Delta T = 3$ K.

- (2011).
- [3] J. Goodenou, *Journal of Solid State Chemistry* **3**, 490 (1971).
- [4] F. J. Morin, *Physical Review Letters* **3**, 34 (1959).
- [5] S. Chandra, D. Franklin, J. Cozart, A. Safaei, and D. Chanda, *ACS Photonics* **5**, 4513 (2018).
- [6] K. Appavoo and J. Haglund, Richard F., *Nano Letters* **11**, 1025 (2011).

- [7] M. J. Dicken, K. Aydin, I. M. Pryce, L. A. Sweatlock, E. M. Boyd, S. Walavalkar, J. Ma, and H. A. Atwater, *Optics Express* **17**, 18330 (2009).
- [8] G. Stefanovich, A. Pergament, and D. Stefanovich, *Journal of Physics-Condensed Matter* **12**, 8837 (2000).
- [9] A. Cavalleri, C. Toth, C. W. Siders, J. A. Squier, F. Raksi, P. Forget, and J. C. Kieffer, *Physical Review Letters* **87**, 237401 (2001).
- [10] M. Rini, Z. Hao, R. W. Schoenlein, C. Giannetti, F. Parmigiani, S. Fourmaux, J. C. Kieffer, A. Fujimori, M. Onoda, S. Wall, and A. Cavalleri, *Applied Physics Letters* **92**, 181904 (2008).
- [11] G. Xu, P. Jin, M. Tazawa, and K. Yoshimura, *Applied Surface Science* **244**, 449 (2005).
- [12] A. Safaei, S. Chandra, A. Vázquez-Guardado, J. Calderon, D. Franklin, L. Tetard, L. Zhai, M. N. Leuenberger, and D. Chanda, *Physical Review B* **96**, 165431 (2017).
- [13] A. S. Barker, H. W. Verleur, and H. J. Guggenheim, *Phys. Rev. Lett.* **17**, 1286 (1966).
- [14] C. Chen, X. Yi, J. Zhang, and B. Xiong, *International Journal of Infrared and Millimeter Waves* **22**, 53 (2001).
- [15] A. Safaei, S. Chandra, M. N. Leuenberger, and D. Chanda, *Acs Nano* **13**, 421 (2019).
- [16] A. Safaei, S. Chandra, M. W. Shabbir, M. N. Leuenberger, and D. Chanda, *Nature Communications* **10**, 3498 (2019).
- [17] M. W. Shabbir and M. N. Leuenberger, *Scientific Reports* **10**, 17540 (2020).
- [18] H. P. Paudel, A. Safaei, and M. N. Leuenberger, in *Nanoplasmonics - Fundamentals and Applications*, edited by G. Barbillon (Intech, London, 2017) Chap. 3, p. 1142.
- [19] P. U. Jepsen, B. M. Fischer, A. Thoman, H. Helm, J. Y. Suh, R. Lopez, and R. F. Haglund, *Phys. Rev. B* **74**, 205103 (2006).
- [20] L. A. L. de Almeida, G. S. Deep, A. M. N. Lima, I. A. Khrebtov, V. G. Malyarov, and H. Neff, *Applied Physics Letters* **85**, 3605 (2004).
- [21] M. M. Qazilbash, M. Brehm, G. O. Andreiev, A. Frenzel, P. C. Ho, B.-G. Chae, B.-J. Kim, S. J. Yun, H.-T. Kim, A. V. Balatsky, O. G. Shpyrko, M. B. Maple, F. Keilmann, and D. N. Basov, *Physical Review B* **79**, 075107 (2009).
- [22] X. Zhong, X. Zhang, A. Gupta, and P. LeClair, *Journal of Applied Physics* **110**, 084516 (2011).
- [23] S. Samanta, A. K. Raychaudhuri, X. Zhong, and A. Gupta, *Physical Review B* **92**, 195125 (2015).
- [24] J. Ordóñez-Miranda, Y. Ezzahri, K. Joulain, J. Drevillon, and J. J. Alvarado-Gil, *Physical Review B* **98**, 075144 (2018).
- [25] W. Guo, Z. Dong, Y. Xu, C. Liu, D. Wei, L. Zhang, X. Shi, C. Guo, H. Xu, G. Chen, L. Wang, K. Zhang, X. Chen, and W. Lu, *Advanced Science* **7**, 1902699 (2020).
- [26] X. Xu, X. He, H. Wang, Q. Gu, S. Shi, H. Xing, C. Wang, J. Zhang, X. Chen, and J. Chu, *Applied Surface Science* **261**, 83 (2012).